Article

Selective Adsorption of Cesium by Supramolecular Materials Loaded with Different Carriers

Jiatian Su[1], Lei Xu[2] and Anyun Zhang[1,*]

[1] College of Chemical and Biological Engineering, Zhejiang University, 866 Yuhangtang Road, Hangzhou 310027, China

[2]

* Correspondence: zhangay@zju.edu.cn (Anyun Zhang)

Abstract: The adsorption of supramolecular composites for Cs(I) in high level liquid waste (HLLW) are different due to different carriers. We chose 25,27-bis(ethyl)-calix[4]arene-26,28-crown-6 (EC[4]C6) as adsorbent, SiO2-P, XAD-7 and UiO-66 as carriers. The synthesis and characterization of supramolecular EC[4]C6 loaded with three different carriers were presented. SEM, N2 adsorption/desorption isotherms, TG-DSC spectra, FT-IR spectra results shown that EC[4]C6 was successfully introduced into the pores of carriers via physical intermolecular interactions. EC[4]C6/SiO2-P, EC[4]C6/XAD-7 and EC[4]C6/UiO-66 shown high efficiency, high selectivity towards Cs(I) over 18 typical fission or corrosion products in HNO3 solution. The adsorption properties of the three materials were investigated after electron irradiation. These results demonstrate that EC[4]C6/SiO2-P possess greater potential for highly efficient removal of Cs(I) from HLLW.

Keywords: calixcrown; carrier; cesium; adsorption; comparision

1. Introduction

Nuclear energy has the characteristics of safety, cleanliness, sustainable and high efficiency[1]. But with the development of nuclear energy, the efficient disposal of nuclear waste has been one of the focuses of nuclear science and technology and one of the difficulties in technical operation[2,3]. There are two types of nuclides Cs, 135Cs and 137Cs in HLLW[4]. There half-lives are 2 million years and 30.2 years. 135Cs has a longer half-life, and it is easy to migrate and has a great potential harm to the environment. Half-life of 137Cs is shorter, but it can release gamma rays and generate a lot of heat, so it is considered to be one of the harmful nuclides which can affect the safety of HLLW glass solidification [5-7]. If the radioactive Cs(I) can be separated, it can not only reduce the volume of glass solidification, shorten the cooling time of waste liquid and the storage life of waste[8,9], but also beneficial to simplify the operation and save costs in geological disposal because of the reduction of heat release[10-12].

Calixarene, as the third generation host molecule[13], has very good pre-organized structure, some of its derivatives have strong ionic special ability[14-16]. Such as partical cone conformation 1,3-dialkoxy-p-spectert-butyl calix[4]-crown-5 can form stable complexes with K(I)[17,18], it can be used as a carrier to support the liquid film. 1,3-alternating conformation 1,3-dialkoxy-p-tert-butyl calix[4]-crown-6 has very strong recognition ability on Cs(I)[19-21]. With the in-depth study of the third generation host molecules, it has been found that the application of calixcrown ethers in the treatment of HLLW has an attractive prospects[22]. Based on the excellent Cs(I) recognition ability of crown ether, researchers at home and abroad have proposed some processes for the treatment of wastewater containing Cs(I)[23], such as the CCCEX process of the French Atomic Energy Agency[24], the CSSX process of Oak Ridge National Laboratory[25], the FPEX

 doi:10.20944/preprints202211.0492.v1

process of Argonne National Laboratory[26], SPEC process proposed by Zhang A[27]. Precipitation, ion exchange and adsorption, liquid-liquid solvent extraction, ionic liquid, extraction chromatography, electrochemical method, membrane, and other methods had been investigated for cesium separation[28,29]. Among them, the adsorption method has the advantages of high removal efficiency, simple operation and low cost[30]. The grafting or impregnation of crown ethers or calixcrown derivatives into various solid materials for cesium adsorption has been studied. The solid supports that have been studied more in recent years are roughly divided into three categories: inorganic supports, organic supports, organic-inorganic composite supports[31,32]. The macroporous silicon-based carrier SiO2-P and resin-based carrier XAD-7 have been reported that they have certain adsorption properties for Cs(I). For example, a macroporous silica-based (Calix[4]+Dodecanol)/SiO2-P adsorbent was prepared, the adsorbent showed a relatively large adsorption capacity of Cs(I) under the gamma-ray field[33,34]. CBC/XAD-7 was prepared by introducing CBC into XAD-7, the adsorbent had a selective recognition effect on Cs(I) and good reusability[35]. MOFs and their related composites exhibited high uptake ability for some radioactive metals[36-38]. Limited results shown that MOFs have a certain adsorption capacity for Cs(I) at low acidity[39,40]. On the condition of high acidity, there were a few studies, for example, MOFs-based adsorbent UiO-66@iPCC5 can separate Rb(I) and K(I) from Cs-effluent[41]. Compared with the existing silicon-based materials and XAD-7-based materials, the adsorption capacity and selectivity of MOFs-based materials on Cs(I) is not clear[42,43], It is necessary to study it further.

To separate Cs(I) form the high acidity solution, three new adsorption materials EC[4]C6/SiO2-P, EC[4]C6/XAD-7 and EC[4]C6/UiO-66 were prepared. They were performed by embedding EC[4]C6 into the pores of the three carriers. The effects of acidity and contact time were investigated to compare the performance of the three materials. The TOC content and irradiation stability experiment were used to evaluate the stability of these materials.

2. Materials and Methods

2.1. Materials and reagents

EC[4]C6 as shown in Figure 1 was provided by Argonne National Laboratory. The silicon-based carrier SiO2-P was developed in our laboratory. The polar carrier XAD-7 containing polyalkyl ester was provided by Sigma-Aldrich. The synthesis of UiO-66 was referenced in the previous literature[44-46]. A nitrate solution containing 19 metal ions was used to simulate HLLW, The metals in this solution were alkali metals(Li, Na, K, Rb and Cs), alkaline-earth metals(Mg, Ca, Sr and Ba), transition metals(Fe, Co, Ni, Ru, Pd, Mo and Zr) and rare earths(Y, La and Nd).

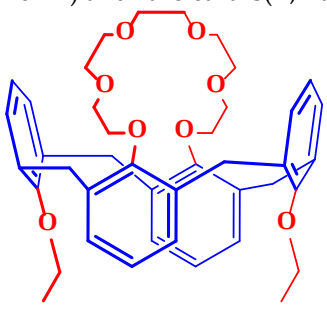

Figure 1. Molecular structures of EC[4]C6.

2.2. Preparation of materials

Silicon-based supramolecular composites EC[4]C6/SiO2-P was prepared by immobilization and vacuum activated perfusion using SiO2-P as the carrier. Specific methods are as follows: the EC[4]C6 and the activated carrier XAD-7 dissolved in a round bottom flask filled with dichlormethane according to the mass ratio of 1: 4, mixed thoroughly in the

Preprints (www.preprints.org) | NOT PEER-REVIEWED | Posted: 28 November 2022 doi:10.20944/preprints202211.0492.v1

rotary evaporator. The EC[4]C6 molecules entered the pores and channels of SiO2-P by diffusion and were bound together by intermolecular interactions. After the removal of dichlormethane by evaporation under reduced pressure, a white powder solid was obtained by vacuum drying. The other two adsorbents (EC[4]C6/XAD-7、EC[4]C6/UiO-66) were got as the same method as above. The technical process of preparation is shown in Figure 2.

Figure 2. Preparation process of adsorbents.

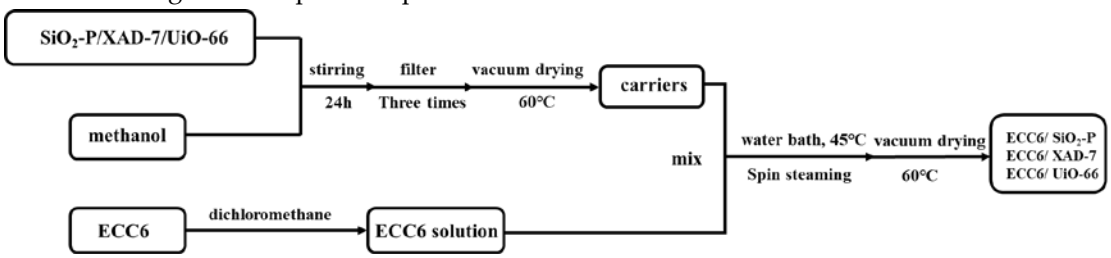

2.3. Adsorption experiment

A series of experiments were conducted to investigate the adsorption selectivity and stability of three kinds of adsorbent materials for Cs(I). The HNO3 solution containing 19 kinds of metal ions was prepared by dissolving the corresponding metal nitrate with concentrated HNO3, the concentration of metal ions was 0.5 mM. 0.1 g of supramolecular recognition materials were used as the solid phase, the aqueous phase was 5.0 mL, 0.5 mM HNO3 solution containing 19 metal ions. The experiment was carried out in MM-10 model thermostated water bath shaker (TAITEC, Japan). The concentration of HNO3 in the water phase varied from 0.4 to 6.0 M, and the contact time varied from 0 to 300 min. The concentration of alkali metal ions in the aqueous phase was determined by AA-240 FS atomic absorption spectrometer (Varian, Inc.), and the concentration of other metal ions in the aqueous phase was determined by 730-ES inductively coupled plasma emission spectrometer (Varian, Inc.). TOC content in aqueous solution after adsorption was determined by 5000 model TOC-VCPN analyzer (Shimadzu, Japan). Distribution coefficient (Kd) and separation factor (SF) were used to evaluate the adsorption performance of adsorption materials on Cs(I) and typical coexisting metal ions. The calculation formula are as follows:

$$K_d = \frac{C_0 - C_e}{C_e} \times \frac{V}{W} \quad (1)$$

$$SF_{A/B} = \frac{K_{d(A)}}{K_{d(B)}} \quad (2)$$

Where, C0 (mM) and Ce (mM) denote the initial and equilibrium concentrations of metal ions in the aqueous phase, respectively. V (cm3) and W (g) are the volume of the aqueous phase and the mass of the supramolecular recognition material, respectively. Kd(A) and Kd(B) represent the adsorption partitioning coefficients of supramolecular recognition materials for metal ions A and B, respectively.

2.4. Irradiation experiment

The three adsorbents were divided into four groups, and the electron irradiation treatment was carried out by high energy electron linear accelerator (CIAE-FZ-10/15). The irradiation dose was controlled by the irradiation time. The irradiation dose of each adsorbent material was divided into: 25, 50, 75 and 100 kGy, the schematic diagram of electron irradiation experiment is shown in Figure 3. Then, the adsorption performance of irradiated adsorption materials was investigated under the optimal acidity, then the adsorption capacity, selectivity of the adsorbents and the change of TOC content in the aqueous phase after adsorption were evaluated.

Preprints (www.preprints.org) | NOT PEER-REVIEWED | Posted: 28 November 2022 doi:10.20944/preprints202211.0492.v1

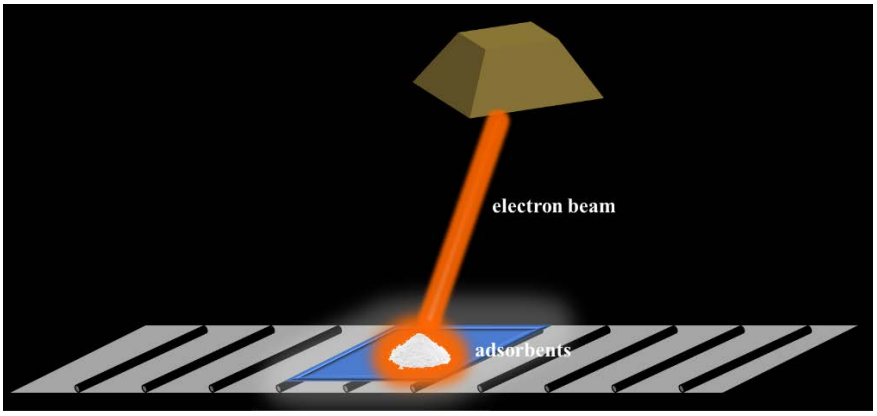

Figure 3. Electron irradiation of adsorbents.

3. Results

3.1. SEM

The micro-morphology and structure of the three carriers and composite materials were observed with the emission scanning electron microscope(SEM). In order to improve the conductivity of the samples, the gold spraying treatment was carried out for 60 s. The characterization results are shown in Figure 4. SiO2-P was a microsphere with the diameter of 40-60 μm, XAD-7 was a macroporous resin structure, and UiO-66 has a good crystal shape, showing a regular octahedral shape. The three adsorption materials have similar structure to the carrier, not presented structure collapse phenomenon, and have a rich and clear channel structure, supramolecular derivatives were successfully fixed into the carrier channels, it was beneficial for Cs(I) to enter the pore and combine with the adsorbent in the subsequent adsorption process.

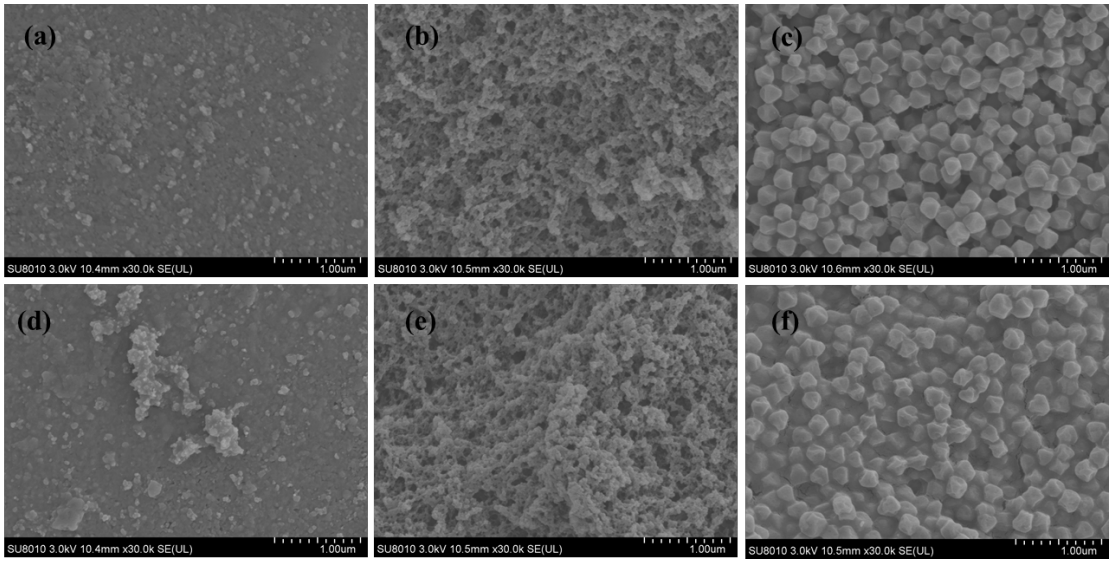

Figure 4. SEM results before and after composition. (a) SiO2-P, (b) XAD-7, (c) UiO-66, (d) EC[4]C6/SiO2-P, (e) EC[4]C6/XAD-7, (f) EC[4]C6/UiO-66.

3.2. N2 adsorption-desorption isotherms

The characterization of N2 adsorption-desorption of the composites are shown in the Figure 5. N2 adsorption-desorption isotherms of EC[4]C6/SiO2-P and EC[4]C6/XAD-7 exhibited a similar type-IV isotherm model (IUPAC classification) with clear steep desorption branch at relative pressures of 0.95-1.0 and a narrow H1 type hysteresis loop,implying the macroporous structure of EC[4]C6/SiO2-P and EC[4]C6/XAD-7, the N2 adsorption-

 doi:10.20944/preprints202211.0492.v1

desorption isotherms of EC[4]C6/UiO-66 exhibited type-I shape which was similar to that of UiO-66 particle. Smaller specific surface and pore volume of the composite materials than these carriers indicated that EC[4]C6 was successfully impregnated into the pores and channels of supports. Some important physical parameters of carriers and adsorbents are listed in Table 1.

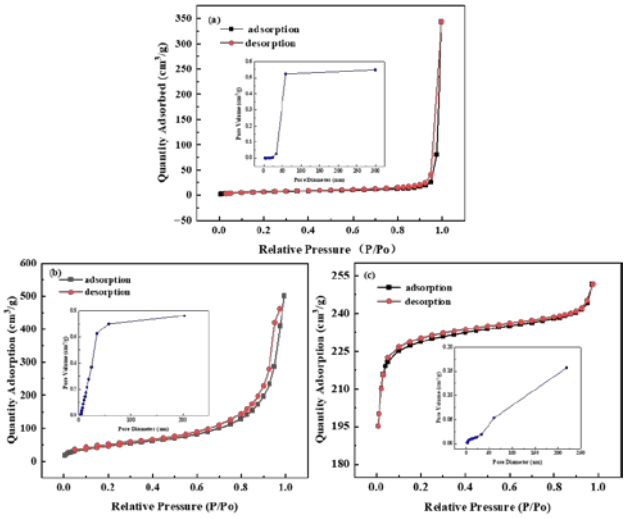

Figure 5. Nitrogen adsorption-desorption isotherms and aperture distribution map. (a) EC[4]C6/SiO2-P, (b) EC[4]C6/XAD-7, (c) EC[4]C6/UiO-66.

Table 1. Structural parameters of the carriers and the adsorbents.

Sample	Specific surface area (m^2/g)	Most probable diameter (nm)	Pore volume (cm^3/g)
SiO_2-P	59.95	60.45	0.8841
EC[4]C6/SiO_2-P	37.23	59.21	0.5486
XAD-7	350.2	34.06	0.7991
EC[4]C6/ XAD-7	165.9	24.28	0.6618
UiO-66	1182	2.079	0.7823
EC[4]C6/ UiO-66	1079	1.836	0.6035

3.3. Thermal analysis (TG-DSC)

In the air atmosphere, the TG-DSC spectra of the three adsorbents were investigated at the temperature range of room temperature to 800 °C at the temperature rate of 10 °C /min, and the results are shown in Figure 6. As can be seen from the figure: In Figure 6 (a), the TG curve had a slight weight change in the temperature range from room temperature to 281.2 °C, and the corresponding exothermic peak appeared in the DSC curve, the main reason was the moisture and residual solvent in the material. Then, with the increase of temperature, the TG curve appeared two obvious weight loss, the weight loss was 13.37% and 12.85% respectively. The corresponding DSC curve shown two exothermic peaks at 357.7 °C and 529.2 °C respectively, indicating that there was a two-step oxidation decomposition of EC[4]C6/SiO2-P, and the oxidation decomposition of polymer in SiO2-P was also included. After the temperature went up to 620 °C, the TG curve basically kept constant weight, and the corresponding DSC curve had no exothermic peak, indicating that EC[4]C6/SiO2-P had been completely oxidized and decomposed, and the weight of inert silicon-based carrier accounted for 70.28%. TG-DSC curve shown that EC[4]C6/SiO2-P owned good thermal stability. In Figure 6 (b), the TG curve appeared a slight weight change in the temperature range from room temperature to 274.9 °C, and the corresponding exothermic peak appeared in the DSC curve. The main reason was the moisture and residual solvent in the material. Later, with the increase of temperature, the TG curve

 doi:10.20944/preprints202211.0492.v1

shown two obvious weight loss, the weight loss was 76.3% and 18.1%, respectively. The corresponding DSC curve also shown two exothermic peaks at 357.1 °C and 465.3 °C respectively, indicating that EC[4]C6/XAD-7 had two-step oxidation decomposition and owned good thermal stability. In Figure 6 (c), the TG curve appeared a slight weight change in the temperature range from room temperature to 100 °C, corresponding to the exothermic peak in the DSC curve, mainly due to the moisture and residual solvents in the material. Later, with the increase of temperature, the TG curve appeared two obvious weight loss, respectively 10.36% and 45.75%, and the corresponding DSC curve also shown two exothermic peaks at 344.6 °C and 541.2 °C, indicating that the EC[4]C6/UiO-66 had a two-step oxidation decomposition and owned good thermal stability.

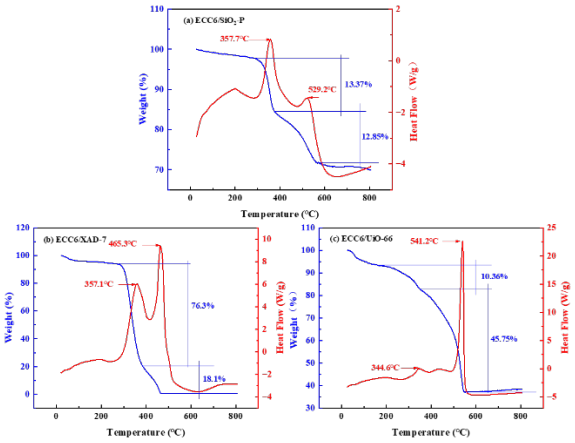

Figure 6. TG-DSC curves of composite materials. (a) EC[4]C6/SiO2-P, (b) EC[4]C6/XAD-7, (c) EC[4]C6/UiO-66.

3.4. FT-IR spectra

At room temperature, FT-IR of the three materials were investigated by KBr laminating method in the range of 4000 cm-1 - 500 cm-1 wave number, and the results are shown in Figure 7. In Figure 7 (a), the characteristic peaks at 1104 cm-1 and 805 cm-1 corresponded to the asymmetric stretching vibration of Si-O-Si. Symmetric stretching vibration indicated that the original structure of carrier SiO2-P was not damaged during the preparation of EC[4]C6/SiO2-P. The characteristic peak at 1457 cm-1 and 2925 cm-1 corresponded to the flexure vibration and stretching vibration of C-H bond of -CH3 in the supramolecular compound EC[4]C6 respectively, and the characteristic peak at 700 cm-1 corresponded to the stretching vibration of C-H bond on the benzene ring of EC[4]C6. There were no new chemical bond generated after the combination of supramolecular and carrier. The EC[4]C6 was successfully combined with the carrier SiO2-P. In Figure 7 (b), the characteristic peak at 2971 cm-1 was attributed to the C-H stretching vibration peak on the saturated carbon of XAD-7, the characteristic peak at 1731 cm-1 was attributed to the stretching vibration peak of the carbonyl group in XAD-7, and the characteristic peak at 1153 cm-1 was caused by bending vibration in the C-H plane and C-C single skeleton vibration. The results shown that there were amorphous macroporous structures in XAD-7. The absorption peaks between 1457-761 cm-1 were the bending vibration and tensile vibration of methyl C-H in EC[4]C6. The polymer-based carrier XAD-7 and EC[4]C6/XAD-7 have similar characteristic peaks. There were no new chemical bond formed between the supramolecular compound and the carrier, indicated that the EC[4]C6 and XAD-7 were physically combined. In Figure 7 (c), the characteristic peak at 1403 cm-1 was attributed to the symmetric stretching vibration peak of the carboxyl group of the organic ligand in UiO-66, and the characteristic peak at 1508 cm-1 and 1582 cm-1 were generated by the vibration of the C=C bond in the benzene ring. In addition, the characteristic peak at 552 cm-1 corresponded to the vibration of Zr-O, indicating the successful coordination of metal ions with the organic ligand and the framework structure of UiO-66. The characteristic peaks between 1575-665 cm-1 were the bending vibration and

 doi:10.20944/preprints202211.0492.v1

tensile vibration of methyl C-H in EC[4]C6. UiO-66 and EC[4]C6/UiO-66 have similar characteristic peaks, and no new characteristic peaks were generated after combination, indicating that EC[4]C6 has been physically combined with carrier UiO-66.

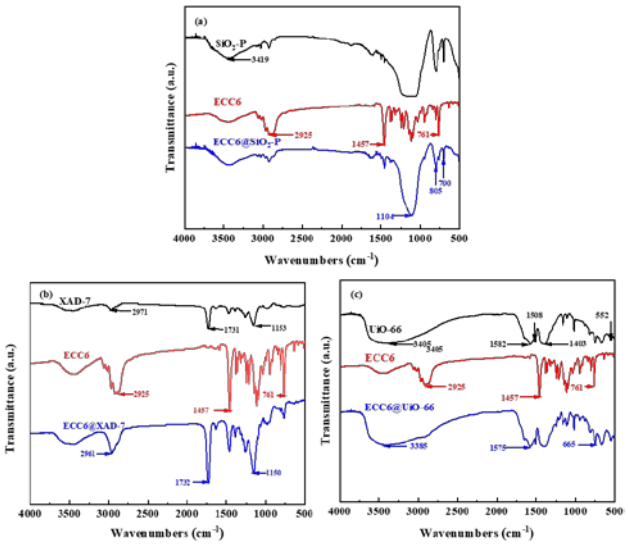

Figure 7. FT-IR spectra of materials before and after composited. (a) EC[4]C6/SiO2-P, (b) EC[4]C6/XAD-7, (c) EC[4]C6/UiO-66.

4. Discussion

4.1. Effect of HNO3 concentration

The concentration of nitric acid in the HLLW was about 3 M. In order to investigate the adsorption feasibility of the three materials on Cs(I) under the condition of high acidity and compare the influence of the different carriers on the adsorption capacity, the influence of the change of HNO3 concentration on the adsorption performance was studied under the condition that the concentration of HNO3 varied from 0.4 to 6.0 M, the result is shown in Figure 8.

In Figure 8 (a), when the concentration of HNO3 increased from 0.4 to 3.0 M, Kd(Cs) increased from 47.45 to 255.46 cm3/g, indicating that increasing the concentration of HNO3 in the range of 0.4-3.0 M was conducive to the adsorption of Cs(I). When the concentration of HNO3 increased from 3.0 to 6.0 M, H+ in HNO3 combined with EC[4]C6/SiO2-P in the form of hydrogen bond, and this process played a dominant role in the competitive reaction, and competed with Cs(I) for the adsorption site on EC[4]C6/SiO2-P. Kd(Cs) decreased from 255.5 cm3/g at 3.0 M to 32.94 cm3/g at 6.0 M. In Figure 8 (b), when the concentration of HNO3 increased from 0.4 to 2.0 M, Kd(Cs) increased from 172.1 to 231.1 cm3/g. As the concentration of HNO3 increased, Kd(Cs) continued to decline, reaching 22.55 cm3/g at 6.0 M. The results shown that after the concentration of HNO3 at 2.0 M, the hydrogen bonding mode between H+ in HNO3 and EC[4]C6/XAD-7 was dominant, and 2.0 M was the best adsorption acidity. In Figure 8 (c), the optimal adsorption acidity of EC[4]C6/UiO-66 for Cs(I) was 3.0 M, and the Kd(Cs) was 103.8 cm3/g. In summary, the three adsorption materials all have certain adsorption capacity for Cs(I) in the environment of high acidity, these results indicated that the three composites were feasible for the adsorption of Cs(I) in HLLW, but their Kd(Cs) were different due to the different carrier loads.

In addition, for other co-existing metal ions, the three adsorbents have weak or even no adsorption on them. In Figure 8 (a), EC[4]C6/SiO2-P had weak adsorption capacity for Rb(I) and K(I). When the optimal adsorption acidity was 3.0 M, Kd(Rb) was 19.53 cm3/g,

 doi:10.20944/preprints202211.0492.v1

Kd(K) was 10.23 cm3/g, but there was no adsorption for other alkaline earth metal ions, transition zone metal ions and rare earth metal ions. In Figure 8 (b), Kd(Rb) was 35.57 cm3/g and Kd(K) was 14.34 cm3/g when the optimal acidity was 2.0 M, and Kd was basically 0 for other metal ions. In Figure 8 (c), at the optimum acidity of 3.0 M, Kd(Rb) was 18.88 cm3/g and Kd(K) was 8.025 cm3/g, and there was almost no adsorption effect on other metal ions.

In summary, the three adsorption materials had obvious adsorption effect on Cs(I), the main reason was that supramolecular derivatives and Cs(I) had a better host and guest recognition function, while Rb(I) and K(I) were the same alkali metal ions as Cs(I), and their sizes were similar to Cs(I), so they had a certain adsorption effect, but EC[4]C6 had little coordination recognition ability for other metal ions. In addition, the chemical properties of rare earth elements were similar, and there was no adsorption on Y(III), La(III) and Nd(III), which further indicated that the composite had no adsorption on other rare earth elements. The adsorption materials would have not only the adsorption feasibility but also good selectivity for Cs(I) in HLLW.

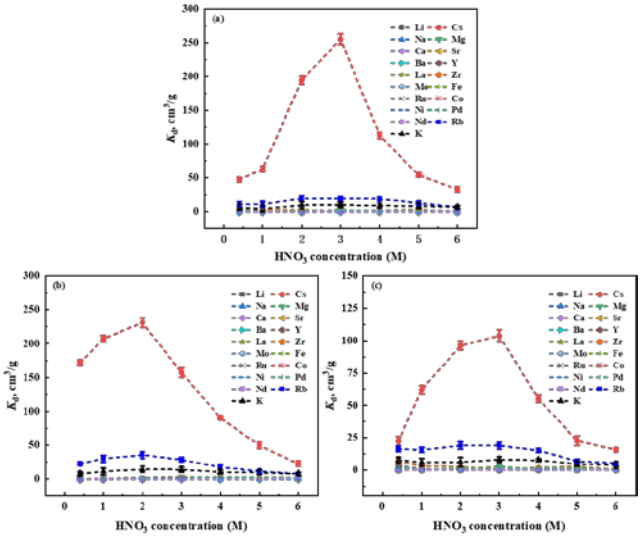

Figure 8. Effect of HNO3 concentration on adsorption properties. (a) EC[4]C6/SiO2-P, (b) EC[4]C6/XAD-7, (c) EC[4]C6/UiO-66.

4.2. Effect of contact time

A series of experiments were conducted to investigate the influence of contact time change on the adsorption performance of the adsorbents. In the experiments, the solid-liquid ratio was 0.1 g/5 cm3, the concentration of HNO3 was the optimal adsorption acidity corresponding to each adsorbent, the temperature was 298 K, the oscillation frequency was 120 rpm, and the contact time varied from 0 to 300 min, results are shown in Figure 9. In Figure 9 (a), Kd(Cs) increased significantly and then became balanced gradually with the extension of time. Kd(Cs) increased from 157.8 cm3 /g at 5 min to 250.1 cm3 /g at 180 min, indicating that the adsorption of Cs(I) by EC[4]C6/SiO2-P could reach equilibrium within 180 min. In addition, EC[4]C6/SiO2-P also exhibited a similar adsorption equilibrium for Rb(I) and K(I). When the equilibrium was reached, the Kd(Rb) was 19.53 cm3/g, Kd(K) was 8.883 cm3/g, but the EC[4]C6/SiO2-P had no adsorption capacity for other 16 metal ions. In Figure 9 (b), Kd(Cs) was 153.1 cm3/g at 5 min, and gradually reached adsorption equilibrium at 180 min, with Kd(Cs) being 229.3 cm3/g. The Kd of Rb(I) and K(I) at equilibrium were 33.61 cm3/g and 12.48 cm3/g, respectively. In Figure 9 (c), the adsorption of EC[4]C6/UiO-66 on Cs(I), Rb(I) and K(I) reached equilibrium at 180 min, Their Kd were 101.6 cm3/g, 18.91 cm3/g and 9.621 cm3/g, respectively. The above

 doi:10.20944/preprints202211.0492.v1

results shown that the adsorption of 19 metal ions by the three materials basically reached equilibrium at 180 min. They had adsorption effect on Cs(I), Rb(I) and K(I), but had almost no adsorption effect on the other 16 metal ions. Among the three adsorption materials, EC[4]C6/SiO2-P had the strongest adsorption capacity for Cs(I). On the one hand, SiO2-P provided regular pore structure for supramolecular derivatives, so that EC[4]C6 could fully entered the pore and combined with SiO2-P through physical interaction, providing conditions for efficient adsorption of Cs(I). On the other hand, SiO2-P had better acid resistance, enabling it to maintain structural stability under high acidity conditions.

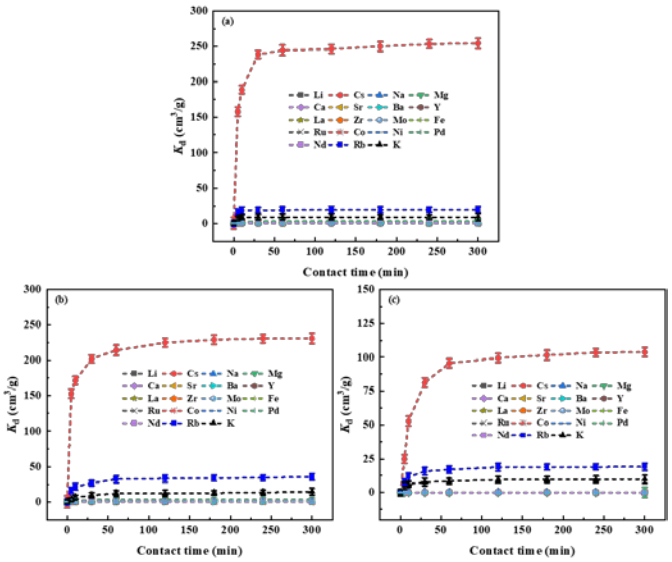

Figure 9. Effect of contact time on adsorption properties. (a) EC[4]C6/SiO2-P, (b) EC[4]C6/XAD-7, (c) EC[4]C6/UiO-66.

4.3. Adsorption isotherm

The isothermal adsorption experiment was carried out to explain the adsorption mechanism and obtain the adsorption capacities. The experiment was carried out under the optimum acidity, contact time of 180 min and 298 K, the initial concentration of Cs(I) varied from 5×10-4 to 0.2 M. Two classical adsorption models described by formula (3) and (4), which denoted the Langmuir and Freundlich models respectively. Langmuir model as presented in formula (3) was usually applicable for the adsorption onto a homogeneous surface with a finite number of identical adsorption sites, while Freundlich model as shown in formula (4) was used to evaluate both monolayer and multi-layer adsorption on a hetergeneous surface.

$$\frac{C_e}{q_e} = \frac{1}{K_L \cdot q_m} + \frac{C_e}{q_m} \tag{3}$$

$$\ln q_e = \ln K_F + \frac{1}{n} \ln C_e \tag{4}$$

In where, Ce denotes the equilibrium concentration of Cs(I) (mM), qe shows the equilibrium adsorption capacity (mM/g), qm represents the monolayer adsorption capacity (mM/g), KL and KF are the constant of Langmuir and Freundlich constant, respectively, 1/n is the heterogeneity factor. The relevant isotherms adsorption parameters of EC[4]C6/SiO2-P, EC[4]C6/XAD-7 and EC[4]C6/UiO-66 are listed in Table 2.

 doi:10.20944/preprints202211.0492.v1

Table 2. Isothermal parameters of the adsorption of Cs(I) onto EC[4]C6/SiO2-P, EC[4]C6/XAD-7 and EC[4]C6/UiO-66.

Adsorbent	Metal ion	$q_{m,exp}$ (mM/g)	Freundlich model			Langmuir model		
			K_F	$1/n$	R^2	K_L	$q_{m,cal}$ (mM/g)	R^2
EC[4]C6/SiO_2-P	Cs(I)	1.126	2.034	0.3623	0.9897	50.81	1.111	0.9931
EC[4]C6/XAD-7	Cs(I)	0.4598	1.148	0.3409	0.9474	198.0	0.4617	0.9958
EC[4]C6/UIO-66	Cs(I)	0.3356	1.631	0.3040	0.9385	102.7	0.3382	0.9999

The results shown that the fitting coefficient R2 obtained according to the Langmuir adsorption model was closer to 1, which was larger than that obtained according to the Freundlich adsorption model, indicating that the adsorption mechanism for Cs(I) was more in line with the Langmuir model. Besides, EC[4]C6/SiO2-P had the largest saturated adsorption capacity among the three adsorption materials, this indicated that SiO2-P was a better carrier than XAD-7 and UiO-66. Supramolecular materials based on silicon were expected to be used for the separation of Cs(I) in HLLW.

4.4. Radiation stability

Although the three materials have certain adsorption capacity of Cs(I) under the condition of high acidity, the adsorption properties of the three adsorbents after irradiation are still unclear, we irradiated the adsorbrnts with electron rays produced by high-energy electron linear accelerator(CIAE-FZ-10/15). Each material was divided into four groups with radiation doses of 25, 50, 75 and 100 kGy, then, we set up batch adsorption experiments on the optimum acidity, 180 min and 298 K. The adsorption experimental data are shown in Figure 10. The stability of the composites was determined by measuring TOC content in aqueous solution.

In Figure 10 (a), with the increasing of irradiation dose, Kd(Cs) decreased from 255.5 to 239.1 cm3/g, the Kd of other metal ions also shown a similar downward trend, at the same time, the corresponding TOC content increased, it shown that electron irradiation reduced the structural stability of supramolecular materials, causing partial EC[4]C6 leakaged into the aqueous phase. In Figure 10 (b), the adsorption performance of the EC[4]C6/XAD-7 also decreased with the increase of irradiation intensity. In Figure 10 (c), the adsorption performance of MOFs-based supramolecular materials decreased significantly after irradiation, the Kd(Cs) was 103.5 cm3/g at 25 kGy and 72.82 cm3/g at 100 kGy, the Kd decreased by 29.6%, it indicated that the stability of MOFs-based adsorbent became worse after irradiation. In summary, after electron irradiation, the adsorption performance of the three materials for Cs(I) decreased, but the adsorption performance of EC[4]C6/SiO2-P decreased less, indicating that its stability was better.

Preprints (www.preprints.org) | NOT PEER-REVIEWED | Posted: 28 November 2022 doi:10.20944/preprints202211.0492.v1

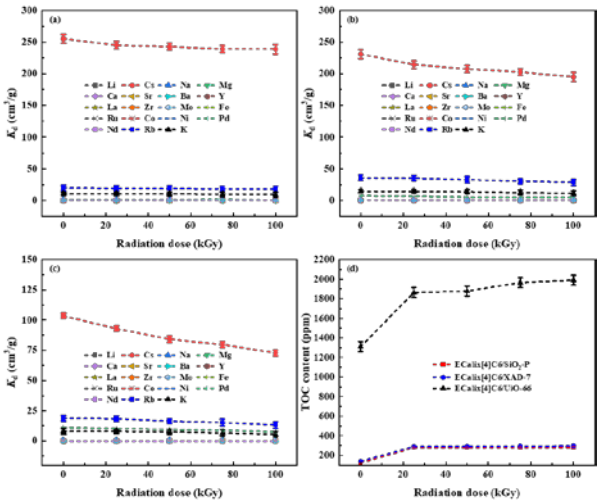

Figure 10. Adsorption performance after irradiation. (a) EC[4]C6/SiO2-P, (b) EC[4]C6/XAD-7, (c) EC[4]C6/UiO-66, (d) changes in TOC content after irradiation.

4.5. Adsorption mechanism

In order to determine the effective adsorption of Cs(I) by supramolecular composites, the XPS and EDS spectra of Cs(I) adsorption were studied. Figure 11 described the XPS spectra of three adsorbents before and after adsorption of Cs(I). The peak at 283.5 eV was ascribed to C 1s binding energy, and the other three peaks located at 531, 744.5, 986.5 eV were attributed to O 1s, O KVV, and C KLL, which were consistent with the elemental composition of the materials. While, there was new peaks at 725 eV after adsorption, it shown that Cs(I) was effectively adsorbed on the three materials. Figure 12 shown the EDS spectra of Cs(I) and Rb(I) after adsorption, there were several peaks at 4.218 keV and 1.837 keV, which were ascribed to Cs(I) and Rb(I) after adsorption, indicating that Cs(I) and Rb(I) were adsorbed, no other elements appeared in the elemental mappings, indicating that the adsorbent adsorbed little or no adsorption on them.

The interaction between calix[4]arene-crown-6 and Cs(I) depended on the of host-guest molecular recognition. Calix[4]arene-crown-6 and Cs(I) can form a relatively stable 1:1 complex[47]. However, under different acidity conditions, adsorbents shown different adsorption properties for Cs(I), which was mainly due to the protonation between HNO3 and adsorption materials through hydrogen bonding, and the competitive adsorption effect was formed between the host and guest recognition and protonation[48].

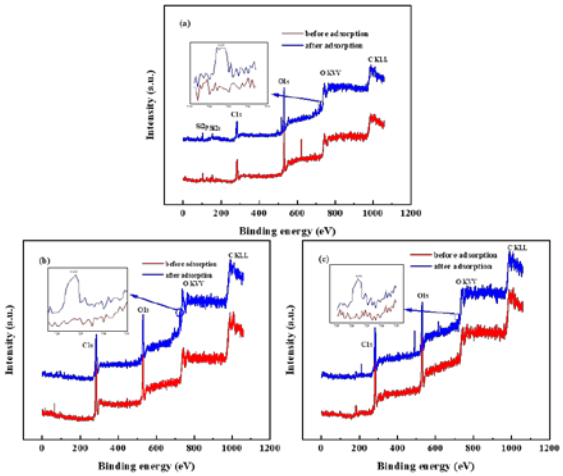

 doi:10.20944/preprints202211.0492.v1

When the concentration of HNO3 is low, the chemical adsorption between Cs(I) and adsorbents is dominant, the complex is [CsEC[4]C6/M]NO3(M = SiO2-P, XAD-7 and UiO-66). With the concentration of HNO3 increasing, H+ in HNO3 will compete with Cs(I) for cavity position in EC[4]C6. The formation of complex was [HEC[4]C6/M]NO3(M = SiO2-P, XAD-7 and UiO-66)[49,50], while, the host-guest molecular recognition was insignificant.

Figure 11. XPS spectra of Cs(I) before and after adsorption. (a) EC[4]C6/SiO2-P, (b) EC[4]C6/XAD-7, (c) EC[4]C6/UiO-66.

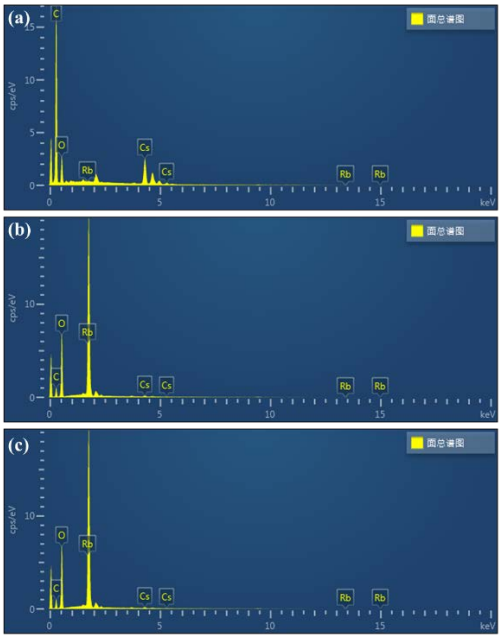

Figure 12. Energy-dispersive X-ray spectra (EDS) of Cs(I) and Rb(I) after adsorption. (a) EC[4]C6/SiO2-P, (b) EC[4]C6/XAD-7, (c) EC[4]C6/UiO-66.

5. Conclusions

HLLW has the characteristics of strong radioactivity and high acid level, its safety treatment has been attached great importance for a long time. The removal of Cs(I) from HLLW is one of these problems. In order to solve this problem, three kinds of supramolecular adsorption materials were prepared, EC[4]C6 was introduced into the pores of the three carriers by immobilized vacuum activated perfusion technology. The adsorption performance of adsorbents with HNO3 concentration between 0.4 and 6.0 M was investigated. EC[4]C6/SiO2-P showed stronger adsorption capacity for Cs(I) among the three materials, and shown weak adsorption or even no adsorption for other co-existing metal ions. The contact time experiment shown that the equilibrium adsorption time of the adsorbents on Cs(I) was 180 min. The isothermal adsorption experimental data were more consistent with the Langmuir model, and the adsorption mode is single molecular layer chemical adsorption. The adsorption performance of adsorbents will decrease under irradiation. Through comparison, it is found that EC[4]C6/SiO2-P has stronger irradiation resistance. The stability of EC[4]C6/SiO2-P and its high selectivity for Cs(I) make it possible to apply in HLLW.

Supplementary Materials: The following supporting information can be downloaded at: www.mdpi.com/xxx/s1, Figure S1: title; Table S1: title; Video S1: title.

Author Contributions: Conceptualization, Anyun Zhang; methodology, Anyun Zhang and Jiatian Su; experiment and characterization, Jiatian Su and Lei Xu; supervision and resources, Anyun

Zhang and Lei Xu; writing and revision, Anyun Zhang and Jiatian Su. All authors have read and agreed to the published version of the manuscript..

Funding: This work was financially supported by National Natural Science Foundation of China (No. U1832124).

Data Availability Statement: Data can be found in the manuscript

Acknowledgments: We are thankful to the Institute of Nuclear-Agricultural Science, Zhejiang University

Conflicts of Interest: The authors declare no conflict of interest

References

1.
2. References
3. 1. Koning, A.J.; Rochman, D. Towards sustainable nuclear energy: Putting nuclear physics to work. Ann. Nucl. Energy 2008, 35, 2024-2030.
4. 2. Wolde-Rufael, Y.; Menyah, K. Nuclear energy consumption and economic growth in nine developed countries. Energy Econ. 2010, 32, 550-556.
5. 3. Kim, Y.; Kim, M.; Kim, W. Effect of the fukushima nuclear disaster on global public acceptance of nuclear energy. Energy Policy 2013, 61, 822-828.
6. 4. Kim, H.; Kim, S.; Hyeon, S.; Kang, H.H.; Lee, K. Application of desalination membranes to nuclide (Cs, Sr, and Co) separation. ACS Omega 2020, 5, 20261-20269.
7. 5. Wang, X.; Shan, T.; Pang, S. Removal of Sr, Co, and Mn from seawater by sargassum horneri in mono- and multi-nuclide contamination scenarios. J. Appl. Phycol. 2021, 33, 2587-2596.
8. 6. Men, W.; Deng, F.; He, J.; Yu, W.; Wang, F.; Li, Y.; Lin, F.; Lin, J.; Lin, L.; Zhang, Y.; Yu, X. Radioactive impacts on nekton species in the northwest pacific and humans more than one year after the fukushima nuclear accident. Ecotox. Environ. Safe. 2017, 144, 601-610.
9. 7. Kim, H.; Kim, M.; Lee, W.; Kim, S. Rapid removal of radioactive cesium by polyacrylonitrile nanofibers containing prussian blue. J. Hazard. Mater. 2018, 347, 106-113.
10. 8. Tao, Y.; Zhenyu, L.; Chunrong, R.; Yuanyuan, W.; Zhichao, H.; Xin, H.; Jie, W.; Mengliang, L.; Qiubai, D.; Khan, K.; Zhongyuan, L.; Shuzhen, L. Study on solidification properties of chemically bonded phosphate ceramics for cesium radionuclides. Ceram. Int. 2020, 46, 14964-14971.
11. 9. Chen, Y.; Jing, Z.; Cai, K.; Li, J. Hydrothermal conversion of Cs-polluted soil into pollucite for Cs immobilization. Chem. Eng. J. 2018, 336, 503-509.
12. 10.Reddy, D.H.K.; Lee, S. Application of magnetic chitosan composites for the removal of toxic metal and dyes from aqueous solutions. Adv. Colloid Interface Sci. 2013, 201-202, 68-93.
13. 11.Gouda, M.M.; Dawood, Y.H.; Zaki, A.A.; Salam Ibrahim, H.A.; El-Naggar, M.R.; Gad, A. Adsorption characteristic of Cs+ and Co2+ ions from aqueous solutions onto geological sediments of radioactive waste disposal site. J. Geochem. Explor. 2019, 206, 106366.
14. 12.Wang, X.; Yu, J. Application of Fe3O4/graphene oxide composite for the separation of Cs(I) and Sr(II) from aqueous solution. J. Radioanal. Nucl. Chem. 2015, 303, 807-813.
15. 13.Basilotta, R.; Mannino, D.; Filippone, A.; Casili, G.; Prestifilippo, A.; Colarossi, L.; Raciti, G.; Esposito, E.; Campolo, M. Role of calixarene in chemotherapy delivery strategies. Molecules 2021, 26, 3963.
16. 14.Ovsyannikov, A.; Solovieva, S.; Antipin, I.; Ferlay, S. Coordination polymers based on calixarene derivatives: structures and properties. Coord. Chem. Rev. 2017, 352, 151-186.
17. 15.Yang, F.; Guo, H.; Vicens, J. Mini-review: calixarene liquid crystals. J. Incl. Phenom. Macrocycl. Chem. 2014, 80, 177-186.
18. 16.Li, P.; Chen, Y.; Liu, Y. Calixarene/pillararene-based supramolecular selective binding and molecular assembly. Chin. Chem. Lett. 2019, 30, 1190-1197.
19. 17.Kang, S.M.; Kim, C.H.; Lee, K.C.; Kim, D.W. Bis-triethylene glycolic crown-5-calix[4]arene: a promoter of nucleophilic fluorination using potassium fluoride. Org. Lett. 2019, 21, 3062-3066.
20. 18.Kim, S.K.; Lynch, V.M.; Young, N.J.; Hay, B.P.; Lee, C.; Kim, J.S.; Moyer, B.A.; Sessler, J.L. KF and CsF recognition and extraction by a calix[4]crown-5 strapped calix[4]pyrrole multitopic receptor. J. Am. Chem. Soc. 2012, 134, 20837-20843.
21. 19.Ramanjaneyulu, P.S.; Kumar, A.N.; Sayi, Y.S.; Ramakumar, K.L.; Nayak, S.K.; Chattopadhyay, S. A new ion selective electrode for cesium (I) based on calix[4]arene-crown-6 compounds. J. Hazard. Mater. 2012, 205-206, 81-88.
22. 20.Raut, D.R.; Kandwal, P.; Rebello, G.; Mohapatra, P.K. Evaluation of polymer inclusion membranes containing calix[4]-bis-2,3-naptho-crown-6 for Cs recovery from acidic feeds: Transport behavior, morphology and modeling studies. J. Membr. Sci. 2012, 407-408, 17-26.
23. 21.Ali, S.M.; Joshi, J.M.; Singha Deb, A.K.; Boda, A.; Shenoy, K.T.; Ghosh, S.K. Dual mode of extraction for Cs+ and Na+ ions with dicyclohexano-18-crown-6 and bis(2-propyloxy)calix[4]crown-6 in ionic liquids: density functional theoretical investigation. RSC Adv. 2014, 4, 22911-22925.
24. 22.Mohapatra, P.K.; Ansari, S.A.; Sarkar, A.; Bhattacharyya, A.; Manchanda, V.K. Evaluation of calix-crown ionophores for selective separation of radio-cesium from acidic nuclear waste solution. Anal. Chim. Acta 2006, 571, 308-314.
25. 23.Jagasia, P.; Mohapatra, P.K.; Dhami, P.S.; Patil, A.B.; Adya, V.C.; Sengupta, A.; Gandhi, P.M.; Wattal, P.K. Studies on the radiolytic stability of newly developed solvent systems containing four calix-crown-6 ligands for radio-cesium recovery. J. Radioanal. Nucl. Chem. 2014, 302, 1087-1093.
26. 24.Zhang, A.; Zhang, W.; Wang, Y.; Ding, X. Effective separation of cesium with a new silica-calix[4]biscrown material by extraction chromatography. Sep. Purif. Technol. 2016, 171, 17-25.
27. 25.Delmau, L.H.; Birdwell, J.F.; Mcfarlane, J.; Moyer, B.A.; Oak Ridge National Lab. Ornl, O.R.T.U. Robustness of the cssx process to feed variation: Efficient cesium removal from the high potassium wastes at hanford. Solvent Extr. Ion Exch. 2010, 28, 19-48.

28. 26.Kumari, I.; Kumar, B.V.R.; Khanna, A. A review on UREX processes for nuclear spent fuel reprocessing. Nucl. Eng. Des. 2020, 358, 110410.
29. 27.Zhang, A.; Xiao, C.; Chai, Z. Spec process II. Adsorption of strontium and some typical co-existent elements contained in high level liquid waste onto a macroporous silica-based crown ether impregnated functional composite. J. Radioanal. Nucl. Chem. 2009, 280, 181-191.
30. 28.Wang, J.; Zhuang, S. Cesium separation from radioactive waste by extraction and adsorption based on crown ethers and calixarenes. Nucl. Eng. Technol. 2020, 52, 328-336.
31. 29.Sheha, R.R. Synthesis and characterization of magnetic hexacyanoferrate (II) polymeric nanocomposite for separation of cesium from radioactive waste solutions. J. Colloid Interface Sci. 2012, 388, 21-30.
32. 30.Lammers, L.N.; Bourg, I.C.; Okumura, M.; Kolluri, K.; Sposito, G.; Machida, M. Molecular dynamics simulations of cesium adsorption on illite nanoparticles. J. Colloid Interface Sci. 2017, 490, 608-620.
33. 31.Chen, S.; Hu, J.; Han, S.; Guo, Y.; Belzile, N.; Deng, T. A review on emerging composite materials for cesium adsorption and environmental remediation on the latest decade. Sep. Purif. Technol. 2020, 251, 117340.
34. 32.Galamboš, M.; Magula, M.; Daňo, M.; Osacký, M.; Rosskopfová, O.; Rajec, P. Comparative study of cesium adsorption on dioctahedral and trioctahedral smectites. J. Radioanal. Nucl. Chem. 2012, 293, 829-837.
35. 33.Ito, T.; Xu, Y.; Kim, S.; Nagaishi, R.; Kimura, T. Adsorption behavior and radiation effects of a silica-based (Calix(4)+Dodecanol)/SiO2-P adsorbent for selective separation of Cs(I) from high level liquid waste. Sep. Sci. Technol. 2016, 51, 22-31.
36. 34.Wu, Y.; Kim, S.Y.; Tozawa, D.; Ito, T.; Tada, T.; Hitomi, K.; Kuraoka, E.; Yamazaki, H.; Ishii, K. Study on selective separation of cesium from high level liquid waste using a macroporous silica-based supramolecular recognition absorbent. J. Radioanal. Nucl. Chem. 2012, 293, 13-20.
37. 35.Dai, Y.; Lv, R.; Fan, J.; Zhang, X.; Tao, Q. Adsorption of cesium using supermolecular impregnated XAD-7 composite: isotherms, kinetics and thermodynamics. J. Radioanal. Nucl. Chem. 2019, 321, 473-480.
38. 36.Kumar, V.; Singh, V.; Kim, K.; Kwon, E.E.; Younis, S.A. Metal-organic frameworks for photocatalytic detoxification of chromium and uranium in water. Coord. Chem. Rev. 2021, 447, 214148.
39. 37.Peng, Y.; Huang, H.; Liu, D.; Zhong, C. Radioactive barium ion trap based on metal-organic framework for efficient and irreversible removal of barium from nuclear wastewater. ACS Appl. Mater. Interfaces 2016, 8, 8527-8535.
40. 38.Garai, M.; Yavuz, C.T. Radioactive strontium removal from seawater by a MOF via two-step ion exchange. Chem 2019, 5, 750-752.
41. 39.Chen, D.; Yang, D.; Dougherty, C.A.; Lu, W.; Wu, H.; He, X.; Cai, T.; Van Dort, M.E.; Ross, B.D.; Hong, H. In vivo targeting and positron emission tomography imaging of tumor with intrinsically radioactive metal-organic frameworks nanomaterials. ACS Nano 2017, 11, 4315-4327.
42. 40.Gao, Y.; Feng, M.; Zhang, B.; Wu, Z.; Song, Y.; Huang, X. An easily synthesized microporous framework material for the selective capture of radioactive Cs+ and Sr2+ ions. J. Mater. Chem. A 2018, 6, 3967-3976.
43. 41.Wang, Z.; Zhang, A.; Su, J.; Chen, R. Selective adsorption of potassium and rubidium by metal-organic frameworks supported supramolecular materials. J. Radioanal. Nucl. Chem. 2021, 329, 359-370.
44. 42.Liu, J.; Thallapally, P.K.; Strachan, D. Metal-organic frameworks for removal of Xe and Kr from nuclear fuel reprocessing plants. Langmuir 2012, 28, 11584-11589.
45. 43.Naeimi, S.; Faghihian, H. Performance of novel adsorbent prepared by magnetic metal-organic framework (MOF) modified by potassium nickel hexacyanoferrate for removal of Cs + from aqueous solution. Sep. Purif. Technol. 2017, 175, 255-265.
46. 44.Cao, J.; Yang, Z.; Xiong, W.; Zhou, Y.; Peng, Y.; Li, X.; Zhou, C.; Xu, R.; Zhang, Y. One-step synthesis of Co-doped UiO-66 nanoparticle with enhanced removal efficiency of tetracycline: Simultaneous adsorption and photocatalysis. Chem. Eng. J. 2018, 353, 126-137.
47. 45.Kandiah, M.; Nilsen, M.H.; Usseglio, S.; Jakobsen, S.; Olsbye, U.; Tilset, M.; Larabi, C.; Quadrelli, E.A.; Bonino, F.; Lillerud, K.P. Synthesis and stability of tagged UiO-66 Zr-MOFs. Chem. Mat. 2010, 22, 6632-6640.
48. 46.Vermoortele, F.; Bueken, B.; Le Bars, G.; Van de Voorde, B.; Vandichel, M.; Houthoofd, K.; Vimont, A.; Daturi, M.; Waroquier, M.; Van Speybroeck, V.; Kirschhock, C.; De Vos, D.E. Synthesis modulation as a tool to increase the catalytic activity of metal-organic frameworks: The unique case of UiO-66(Zr). J. Am. Chem. Soc. 2013, 135, 11465-11468.
49. 47.Yi, R.; Xu, C.; Sun, T.; Wang, Y.; Ye, G.; Wang, S.; Chen, J. Improvement of the extraction ability of bis(2-propyloxy)calix[4]arene-crown-6 toward cesium cation by introducing an intramolecular triple cooperative effect. Sep. Purif. Technol. 2018, 199, 97-104.
50. 48.Makrlík, E.; Vaňura, P.; Asfari, Z. Solvent extraction of some univalent cations into nitrobenzene by using cesium dicarbollylcobaltate and four bis(crown-6) ether derivatives of calix[4]arene. J. Solut. Chem. 2019, 48, 445-454.
51. 49.Ho, T.A.; Argyris, D.; Cole, D.R.; Striolo, A. Aqueous NaCl and CsCl solutions confined in crystalline slit-shaped silica nanopores of varying degree of protonation. Langmuir 2012, 28, 1256-1266.
52. 50.Lyu, Y.; Zhang, A.; Wang, Y. Selective adsorption of rubidium onto a new 1,3-alternate calix[4]crown-5 mesoporous adsorbent with a polar carrier containing polyalkyl ester. J. Chem. Eng. Data 2020, 65, 198-208.